COMMUNICATION

Giant Resistive Switching via Control of Ferroelectric Charged Domain Walls

*Linze Li, Jason Britson, Jacob R. Jokisaari, Yi Zhang, Carolina Adamo, Alexander Melville, Darrell G. Schlom, Long-Qing Chen, and Xiaoqing Pan**

Interfaces in strongly correlated systems hold great potential for the development of new device paradigms owing to the unique properties and novel functionalities they can possess with respect to the parent materials. Heterointerfaces separating materials with different chemical compositions have been reported to display many interesting phenomena such as insulator–metal transitions, superconductivity, and magnetism.[1–5] Similar effects are also expected at compositionally homogeneous interfaces, such as boundaries between different domains (domain walls) in ferroics. For example, it has been predicted that boundaries in nonpolar materials can be ferroelectrically polarized;[6] and ferromagnetic domain walls can exist in antiferromagnetic or paramagnetic materials.[7,8] While heterointerfaces are fixed in space, domain walls can be created, erased, and reconfigured within the same physical volume by external magnetic, electric, or strain fields. Domain walls, then, may form the building blocks for reconfigurable nanoelectronic devices.

In ferroelectrics, one intriguing property associated with domain walls is their enhanced conductivity compared to the surrounding domains.[9–15] As ferroelectric domains can be easily written or erased by an external electric field, they may be suitable for novel applications in logic and memory devices. Most observed domain walls are, however, nearly charge-neutral due to a minimization of the electrostatic energy and only slightly enhanced conductivity at such uncharged domain walls has been shown.[9–13] This impedes potential application as the

conductivity is thermally activated and the current is therefore very low. On the other hand, charged domain walls (CDWs) that break polarization continuity have also been observed.[14–19] Such CDWs are electronically active due to the accumulation of bound charge, which may gather compensating free charges and thus allow higher conductivity than uncharged domain walls.

In general, two types of CDWs can be found in proper ferroelectrics.[14] The first type forms when the equilibrium configuration of an uncharged domain wall is perturbed during polarization switching or domain wall bending caused by an external field. These CDWs are weakly charged and show transient, enhanced conductivity $10–10^3$ times that of the bulk.[15] They are usually unstable and tend to relax to low-energy, uncharged orientations after removal of the external field.[16] Although defect pinning can increase the stability of such CDWs, this mechanism relies critically on the local defect microstructure, making these CDWs impractical for reliable, reconfigurable devices. In contrast, the second type forms as a result of direct "head-to-head" or "tail-to-tail" polarization configurations and is stabilized through the compensation of accumulated free charge carriers without defect pinning.[14,17–19] These CDWs are therefore strongly charged and are referred to as strongly charged domain walls (sCDWs). Recent experimental investigations have demonstrated that a quasi-2D electron gas can form at these sCDWs, leading to steady metallic conductivity 10^9 times that of the bulk.[14,20] Consequently, the sCDWs hold more promise for device applications.

Direct manipulation of sCDWs has so far been explored in only a few works in ferroelectric thin films using conventional surface probes such as piezoresponse force microscopy (PFM) and conductive atomic force microscopy.[21,22] Contrary to the dramatically enhanced steady metallic conductivity (10^9 times that of the bulk) measured at sCDWs in bulk crystals of $BaTiO_3$,[14] the observed conductivity at the sCDW in the thin films is only slightly or moderately enhanced ($10–10^3$ times that of the uncharged domains).[21,22] One possible cause is that the sCDWs observed by PFM may be in fact only present at the top surface and do not penetrate to the bottom interface of a film. For example, cross-sectional transmission electron microscopy (TEM) of $BiFeO_3$ thin films showed that a sCDW can form at the film surface as a result of the formation of a triangular charge-neutral nanodomain, with a small size approaching the resolution limit of surface probe microscopy techniques, beneath the surface.[17] These hidden nanodomains associated with the sCDWs could also significantly affect the film conductivity at the local region. Therefore, a study of the dynamic behavior of sCDWs in response to an applied electric field in the cross-section view is critical to understanding emergent

L. Z. Li, Dr. J. R. Jokisaari, Dr. Y. Zhang, Prof. X. Q. Pan
Department of Chemical Engineering and Materials
Science and Department of Physics and Astronomy
University of California - Irvine
Irvine, CA 92697, USA
E-mail: xiaoqing.pan@uci.edu
L. Z. Li, Dr. J. R. Jokisaari, Dr. Y. Zhang
Department of Materials Science and Engineering
University of Michigan
Ann Arbor, MI 48109, USA
Dr. J. Britson, Prof. L.-Q. Chen
Department of Materials Science and Engineering
Penn State University
University Park
PA 16802, USA
Dr. C. Adamo, Dr. A. Melville, Prof. D. G. Schlom
Department of Materials Science and Engineering
Cornell University
Ithaca, NY 14853, USA
Prof. D. G. Schlom
Kavli Institute at Cornell for Nanoscale Science
Ithaca, NY 14853, USA

Makerials
Views
www.MaterialsViews.com

ADVANCED
MATERIALS
www.advmat.de

COMMUNICATION

conductive phenomena associated with sCDWs. Moreover, different types of sCDWs buried beneath the surface[17,23–25] have also been observed by cross-sectional TEM, but direct manipulation of them has been impossible by conventional surface approaches. Here, using a recently developed in situ TEM[26,27] coupled with phase-field simulations, we report the reversible switching of stable nanoscale sCDWs and corresponding nanodomains induced by an electric field applied across the cross sectional sample of an epitaxial BiFeO$_3$ thin film. A dramatic resistive switching is observed as the length of the CDW surpasses a critical value, leading to the highest resistance changes (off/on ratio ≈10^5) ever reported in ferroelectric memories, including ferroelectric tunneling junctions[28–30] and switchable ferroelectric diodes.[31,32]

Local switching was performed upon 20 nm thick (001)$_P$ oriented BiFeO$_3$ (BFO) single crystalline films grown on (110)$_O$ TbScO$_3$ (TSO) substrates with epitaxial 20 nm La$_{0.7}$Sr$_{0.3}$MnO$_3$ (LSMO) bottom electrodes[17,33] (subscripts P and O are used to indicate pseudocubic and orthorhombic indices, respectively). A bias was applied between a tungsten surface probe and the LSMO bottom electrode (**Figure 1**a). In these films, arrays of stable nanoscale sCDWs have been found, with a feature size as small as 10 nm.[17]

A cross-sectional dark-field diffraction contrast TEM image of a system with a stable sCDW is shown in Figure 1b. The polarization configuration within the (100)$_P$ plane (image plane) was unambiguously determined through quantitative mapping of the displacements between the Fe and Bi atoms using atomic-scale high-angle annular dark-field (HAADF) scanning transmission electron microscopy (STEM) imaging,[17] as shown in Figure 1d–g. Because of the small anisotropic strain due to the dissimilar symmetry of (001)$_P$ BiFeO$_3$ and (110)$_O$ TbScO$_3$, only two rhombohedral ferroelastic variants (r$_1$ and r$_4$) can form in the BiFeO$_3$ bulk films grown on TbScO$_3$ substrates, leading to four possible polarization directions: [111]$_P$, [$\bar{1}\bar{1}1$]$_P$, [1$\bar{1}$1]$_P$, and [$\bar{1}$1$\bar{1}$]$_P$.[33] As a result, once the polarization direction within the (100)$_P$ is known, the polarization orientation along the [100]$_P$ axis (zone axis perpendicular to the image plane) can also be determined. Therefore, the vertical and inclined boundaries of the triangular domain in Figure 1b are 109° and 180° domain walls, respectively.

As the tip of the triangular domain is located above the BFO/LSMO interface, a 71° sCDW with "head-to-head" polarization
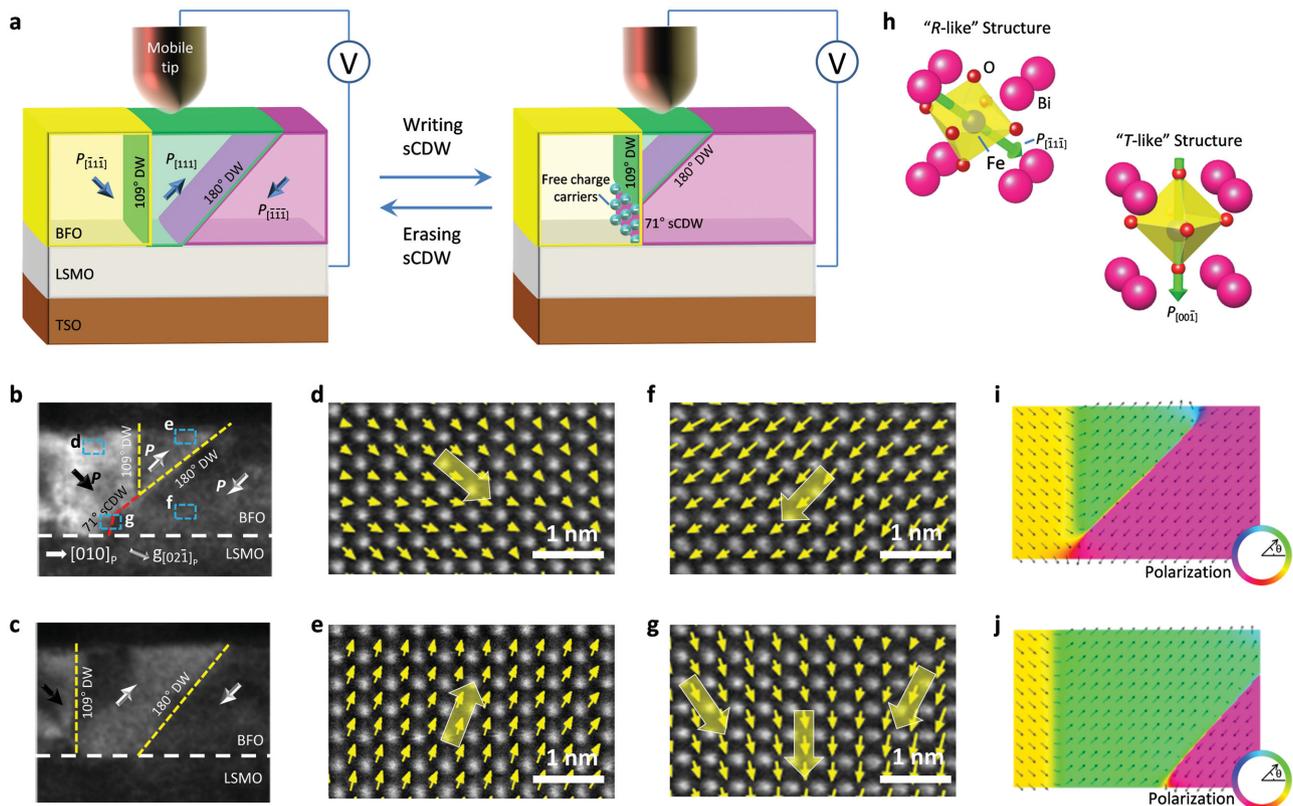

Figure 1. Bistability of the system associated with a sCDW in BiFeO$_3$ thin film. a) Schematic of the experimental set-up: a BFO thin film was grown on LSMO/TSO, and a mobile tungsten tip acts as one electrode for electrical switching with the LSMO layer being grounded. Through the application of an electrical bias, sCDW can be written and erased in the BFO film. b) Cross-sectional dark-field TEM image showing a triangular 109°/180° domain wall (DW) junction with a 71° sCDW. c) TEM image showing a domain configuration of separated 109° and 180° domain walls, without a sCDW. Note that P denotes the polarization directions in the domains. For scale, the BiFeO$_3$ film thickness in (b) and (c) is 20 nm. d–g) High-resolution HAADF STEM image of the four different regions highlighted by the rectangles in (b). Vectors indicate the polarization direction across these regions described. h) Atomic models of the R-like structure of the domains and the T-like structure of the sCDW in BiFeO$_3$. Polarizations are shown by green arrows. i) Phase-field simulation of the polarization distribution in the plane of the image of the stable domain structure with a sCDW in a BFO film. j) Simulated polarization distribution in the plane of the image of the stable domain structure of the system without a sCDW. The arrows mark the polarization orientations. For scale, the BiFeO$_3$ film thickness in (i) and (j) is 19 nm.
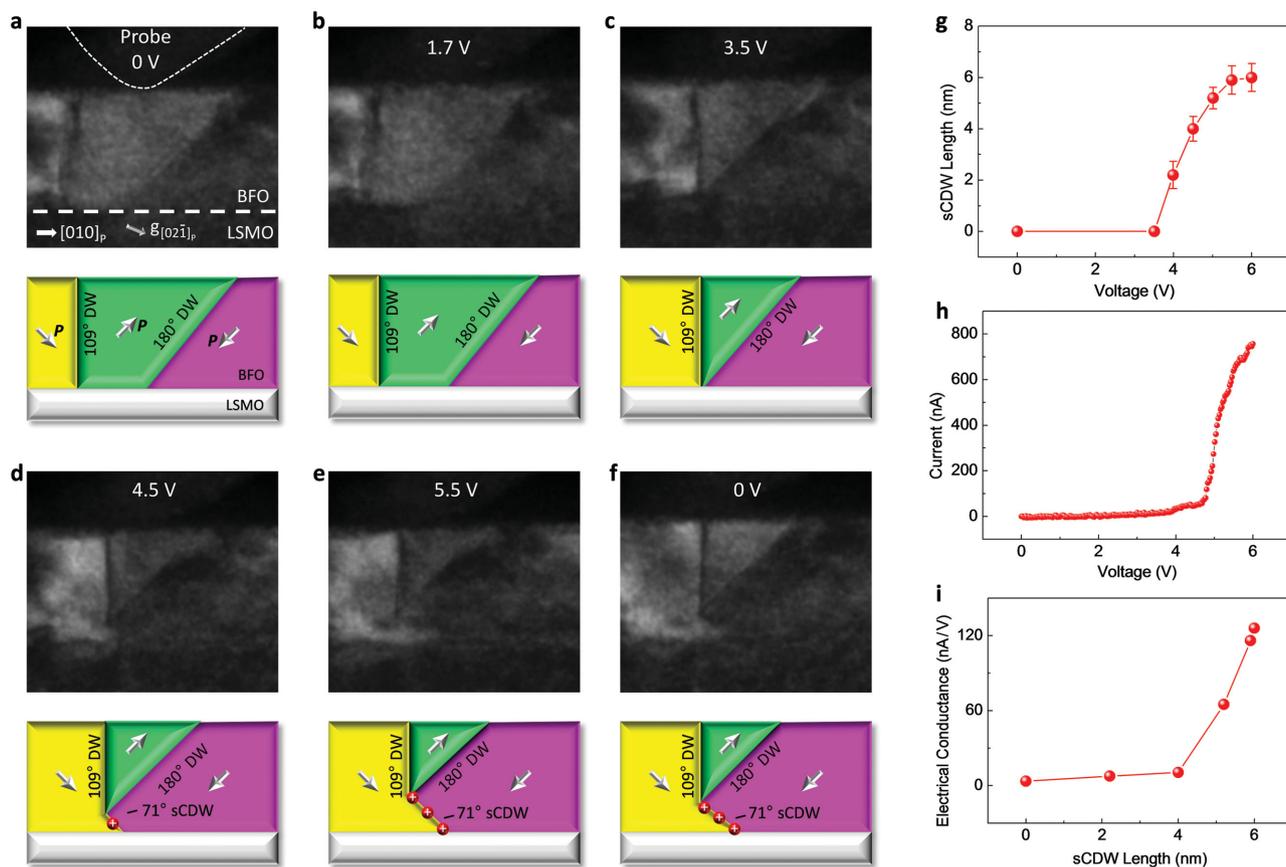
Figure 2. Creation of a sCDW caused by applying a positive ramp bias using in situ TEM. a) The original stable state without a sCDW in the BFO film. b) At the critical bias, the domain wall (DW) started to move. c) The 109° and 180° domain walls intersect at the substrate interface as a result of domain wall motion. d,e) Formation and growth of a sCDW as a result of upward motion of the tip of the triangular 180°/109° domain wall junction. f) After removal of the bias, the sCDW relaxed to be shorter than that observed in (e). For scale, the film thickness is 20 nm. g) The measured length of the sCDW as a function of the applied voltage. h) In situ measured current during the creation of the sCDW. i) The measured local electrical conductance of the film as a function of the sCDW length.

is created there. Interestingly, while the bulk domains possess the rhombohedral-like (R-like, Figure 1h left) perovskite structure with polarization pointing along the body diagonal of the BFO lattice (Figure 1d–f), the polarization near the sCDW has rotated into the direction normal to the BFO/LSMO interface (Figure 1g), forming a tetragonal-like (T-like, Figure 1h right) structure at the local boundary.[17] This structural change is also reproduced by phase-field simulation of the sCDW configuration (Figure 1i). Since the bound charge adjacent to the interface can be compensated by free carriers from the bottom electrode, the system favors formation of the sCDW to reduce the total domain wall area to minimize its electrostatic energy.[17] Note that although the sCDW is inclined here (Figure 1b) we have also observed stable vertical sCDW in the same system,[17] which shows that the most stable configuration of a sCDW can depend on competition between electrostatic and elastic driven forces associated with local charge accumulation and structural transformation. On the other hand, the system can also be stable without a sCDW as shown in the TEM image (Figure 1c) and the simulated result (Figure 1j). In this case the 109° and 180° domain walls are separated by a sufficient distance so that their interaction is weak. From these two sets of observations

and simulations we conclude that the system is bistable and can exist either with or without a sCDW.

A sCDW can be created by applying a bias, as shown in the chronological series of images presented in **Figure 2**a–f. The bias was linearly increased from 0 to 6.0 V over 50 s. The initial stable structure (Figure 2a) contained 109° and 180° domain walls separated by 10 nm at the substrate interface. The onset of domain wall motion occurred at a critical applied bias of 1.7 V (Figure 2b). As larger biases were applied, a two-stage switching process occurred. During the first stage, the two 109° and 180° domain walls moved toward each other until they intersected (Figure 2c). During the second stage, further shrinkage of the triangular domain led to upward motion of the triangular domain tip and resulted in the formation and elongation of a sCDW (Figure 2d,e). The measured length of the sCDW, which is defined as the distance from the triangular domain tip to the BFO/LSMO interface, is plotted as function of applied voltage (Figure 2g). After the bias was removed, the system relaxed to a stable state and the length of the sCDW remained ≈5 nm (Figure 2f).

By measuring the in situ current during the switching process (Figure 2h), we are able to correlate the domain wall

Materials
Views
www.MaterialsViews.com

ADVANCED
MATERIALS
www.advmat.de

COMMUNICATION

configuration and the film conductivity in real time. When the applied voltage is lower than 3.5 V, the film showed almost no conductivity (current < 10 nA, which is approaching the resolution limit of the in situ apparatus), corresponding to domain configurations without a sCDW (Figure 2a–c). When the voltage reaches 4.5 V, the film showed little conductivity (current ≈50 nA), corresponding to domain configurations with only a relatively short sCDW (length ≈4 nm). Further increasing the bias caused the sCDW to elongate, leading to dramatically increased conductivity measurements. Significant conduction with strongly enhanced currents of 640–760 nA occurred at voltages higher than 5.5 V. The resistive switching also shows good repeatability at multiple spots where the same type of sCDW exists (Figure S1, Supporting Information) and is absent during the switching process at local monodomain regions without a sCDW in the same film (Figure S2, Supporting Information). Previous studies have shown that resistive switching in ferroelectric films can occur via a switchable Schottky-to-Ohmic interfacial contact between the electrode and the semiconducting ferroelectric film, and the switching occurs as the sign of polarization bound charge at the interface is reversed.[32,34] In the local region where a sCDW is present in our system, during the resistive switching observed at 4.5–5.5 V (Figure 2d,e), the top BiFeO$_3$/probe interface and the bottom BFO/LSMO interface both have positive polarization bound charge and no change of the sign of the bound charge is observed, excluding a switching between the Schottky and Ohmic contacts at the interface. Since the positive bound charge would attract accumulated compensating electrons (free carriers in n-type BFO) and lead

to downward band bending, both the interfaces of the local film with a CDW would be Ohmic contacts.[32,34] Therefore, the conductivity of the system is primarily dependent on the bulk of the semiconducting BFO film rather than the interfaces. Upon the elongation of the sCDW at 4.5–5.5 V (Figure 2d,e), a very high charge state can be created in the local region, causing the observed significant change of the film conductivity. Combining the measured sCDW length (Figure 2g) and in situ current (Figure 2h) during the switching process, a direct correlation between the electrical conductance of the local film and the sCDW length can be made, as shown in Figure 2i. This correlation shows a nonlinear relation and a substantial enhancement of film conductivity when the sCDW penetrates more than a critical value in length (≈4 nm in this case).

To better understand the formation of the conductive state caused by the sCDW, phase-field modeling (see the Supporting Information for details) of the epitaxial thin film was employed (**Figure 3**). Polarization distributions of three characteristic domain structures, shown in Figure 3a–c, closely resemble the experimentally observed domain configurations shown in Figure 2c–e. In this simulation, Figure 3b, a small T-like sCDW above the bottom interface was found to be the most stable domain configuration. Domain structures starting from either closely spaced 109° and 180° domain walls in which no T-like sCDW exists (Figure 3a) or from a largea sCDW state (Figure 3c) were allowed to relax toward the equilibrium configuration (Figure 3b).

The corresponding calculated electrical potential distributions around the domain walls resulting from the polarization
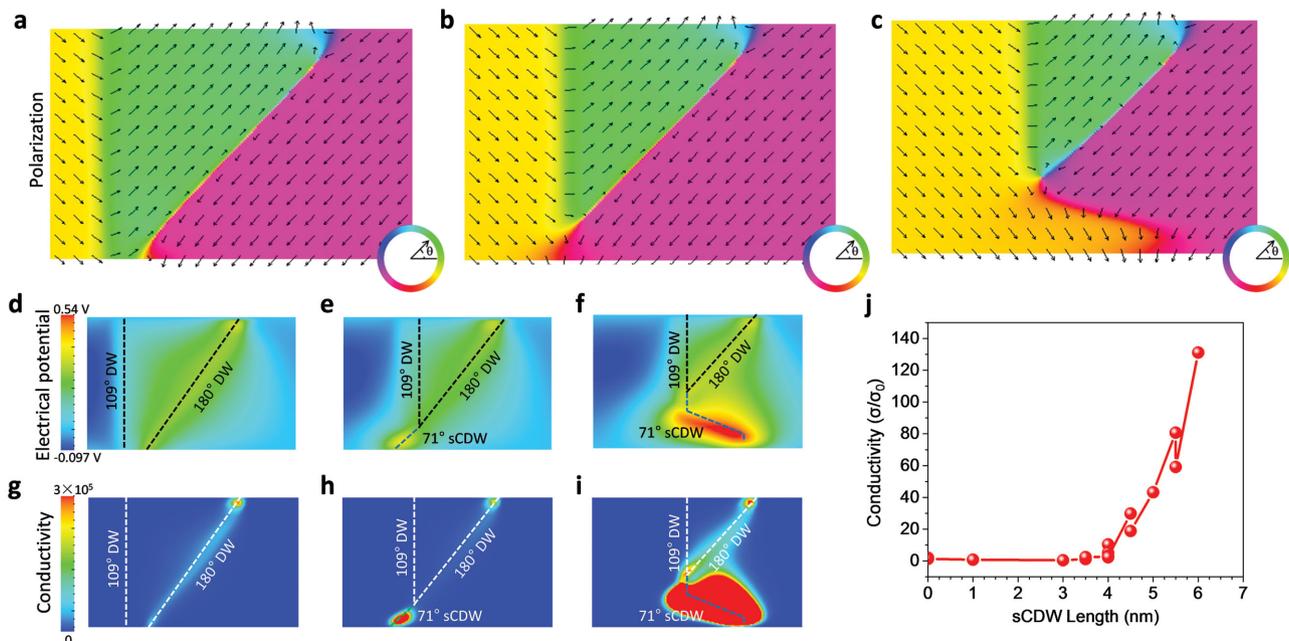

Figure 3. Phase-field simulations of electrical state around a sCDW in a BiFeO$_3$ thin film. a–c) Polarization distributions for metastable domain structures with two closely spaced domain walls with no sCDW (a); a small separation between the triangular domain and electrode with a limited sCDW (b); and a larger sCDW resulting from a large separation between the triangular domain and electrode (c). The arrows mark the polarization orientations. d–f) Electric potential distribution calculated from the polarization bound charges in domain structures (a–c), respectively. g–i) Normalized thin film conductivity around domain structures (a–c). j) Total calculated normalized conductivity of the BFO thin film around the domain structure for a series of charged domain wall lengths (defined as the distances between the triangular domain tip and the bottom electrode). For scale, the film thickness is 19 nm.

bound charge are shown in Figure 3d–f. For the case of closely separated domain walls (Figure 3a,d), the sharper change in the polarization at the nominally charge neutral 180° domain wall leads to a very small electrical potential there, as a result of the thin film boundary conditions. When the sCDW forms (Figure 3b,e), the electrical potential at the boundary is increased due to the larger polarization bound charge. As the sCDW further elongates (Figure 3c,f), the bound charge around the sCDW is significantly increased leading to a distributed area of high electrical potential in the thin film. Although the sCDW only penetrates less than half of the film thickness, an enhanced potential is observed within a much broader region in the film, including a widened region along the inclined 180° domain wall. This observed enhanced potential would attract free charge carriers at local areas, leading to enhanced conductivity not only at the sCDW, but also along the 180° domain wall in the upper portion of the film above the sCDW. As a result, a significant increase of conductivity through the film is achieved by the creation of lower resistance paths through the film along the sCDW and 180° domain wall. These paths along the domain walls effectively act as short-circuit routes for flow of the electrical current.

We used the simulated electrical potential to calculate the expected relative electrical conductivity of the BFO thin films around the sCDW. Since the defect chemistry of BFO is poorly understood, it is difficult to predict the major charge carriers. Previous studies, however, have shown that conductivity at CDWs is typically strongest at "head-to-head" domain walls with positive bound charge, suggesting that, in some films at least, negative charge carriers dominate conduction.[21] Following this assumption, we estimate the negative charge carrier density around the domain walls using Boltzmann statistics and assume the density of positive charge carriers to be negligibly small. The local conductivity is then estimated as

$$\sigma = \sigma_0 \exp\left(-\frac{e\varphi}{k_b T}\right) \tag{1}$$

where

$$\sigma_0 = N_0 e \mu \tag{2}$$

In Equations (1) and (2) above e is the charge on an electron, φ is the electrical potential, k_b is Boltzmann's constant, T is the absolute temperature, N_0 is the background carrier density, and μ is the carrier mobility. The calculated normalized local conductivities are shown in Figure 3g–i. These results show the sCDW is expected to have very large conductivity. This arises from the high carrier concentrations, which can be 10^6 times larger than the background carrier concentration.

The total estimated conductivity through the film around the sCDW and the triangular domain structure was calculated by summing the contributions from all of the individual grid points in the simulated film (from the top surface to the bottom interface), as plotted in Figure 3j. Here we calculated the relative conductivity of the film assuming the simulated film is placed in a capacitor arrangement with conducting electrodes covering the entire top and bottom of the film. Although this simulation approach estimates the total effect of the domain structure

change on the conductivity of the film over a larger volume of the film rather than only under a local electrode, we only allow a change of the sCDW and the triangular domain structure and restrict all other domain structures to be constant during the simulation. Therefore, any calculated change of conductivity should be caused by the local switching of the sCDW. For this analysis it was assumed that the grid points in lines parallel to the substrate conducted in parallel (inverse resistances add) while grid lines along the thickness were in a serial configuration during conduction (resistances add). To find the total film conductivity we first summed each row of grid points that conducted in parallel and then summed the results, which conducted in series. While the order of this operation changed the magnitude of the expected conductivity, it had no effect on the trends in the normalized results. Total calculated normalized film conductivity as a function of the length of the sCDW, which is defined as the distance of the triangular domain tip from the bottom electrode, is plotted in Figure 3j. Note that two data points of conductivity values have been shown at some points of the same length of the sCDW. This is because we repeated the simulations at a few data points with different initial random noise in the system. Not all data points were exactly reproduced, but they generally follow the same trend. Initially, the conductivity of the thin film is very small for small separations between the electrode and triangular domain tip, corresponding to limited formation of the sCDW. For larger sCDW, however, the conductivity is clearly seen to increase rapidly, in good agreement with the experimental results shown in Figure 2i.

The sCDW can also be erased by reversing the applied voltage (linearly decreasing it from 0 to −6.0 V over 50 s), as shown in Figure S3 (Supporting Information). The critical bias to induce domain wall motion in this case (−1.46 V, as shown in Figure S3b (Supporting Information)) was similar in magnitude to that in the sCDW writing process. Switching occurred by growth of the triangular domain (Figure S3c, Supporting Information), exactly reversing the domain shrinkage in the creation process. Finally, the system was returned to the original stable domain structure without a sCDW (Figure S3d, Supporting Information). This state remained stable after removal of the bias (Figure S3e, Supporting Information).

The high stability and the large conductivity difference of the two states examined above, which are interconvertible through reversible switching of the sCDW, enables nondestructive resistive readout with a large off/on ratio. To demonstrate this we applied a "readout" bias sweep, linearly increasing from 0 to 1.5 V, and measured the readout currents for each of the two states (**Figure 4**). This voltage is less than the critical voltage required to move the domain walls and does not change the domain structure of the BFO thin film. The readout $I–V$ curve current for the "on" state with a sCDW shows an Ohmic behavior, further supporting the conclusion of Ohmic contacts at both interfaces of the local film where a sCDW is present. While the readout current for the "on" state reached up to ≈100 nA at $V = 1.50$ V, the readout current for the "off" state without a sCDW appeared to be effectively zero, as any current was less than the noise level (several nanoamperes) of the in situ apparatus. As the "off" state mainly conducts through bulk electrical transport and uncharged domain walls, its readout currents can be estimated by using scanning spreading
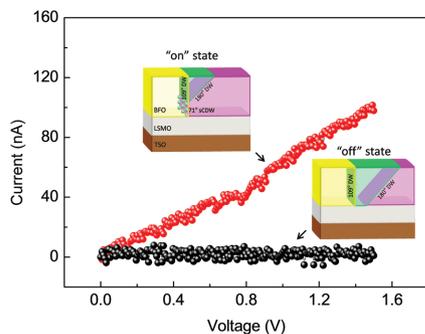
Materials
Views
www.MaterialsViews.com

ADVANCED
MATERIALS
www.advmat.de

COMMUNICATION

Figure 4. Conductivity comparison of the "on" and "off" states in a BiFeO$_3$ thin film. The data points show the in situ measured readout current of the system with ("on" state) and without ("off" state) a sCDW when applying a positive bias ramp from 0 to 1.5 V. The insets show schematics of the domain configurations of the "on" and "off" states. During the measurement, domain wall motion was not observed. Notice that no current except noise was detected for the "off" state.

resistance microscopy (SSRM) with better current resolution. The measured currents of uncharged domain walls and bulk domains in the same film between a surface probe and the LSMO bottom electrode are lower than a few picoamperes (Figure S3, Supporting Information), consistent with previously published results for BiFeO$_3$ thin films.[9,10,13] Consequently, the off/on ratio of the switchable resistivity in the system is determined to be about 10^5. Moreover, the off/on ratio can be in principle increased by choosing thinner ferroelectric films, where the inclined domain wall of the triangular domain above the sCDW can also become charged due to polarization rotation effects observed in this system.[17]

In conclusion, we have demonstrated the reversible switching of stable nanoscale sCDWs in ferroelectric BiFeO$_3$ thin films. Since the "head-to-head" sCDW in rhombohedral-like BiFeO$_3$ thin films observed here possess a tetragonal-like structure, the process of creating or erasing a sCDW in the film would involve a dynamic transition between different lattice symmetries induced by an applied electric field. Significant resistive switching is observed in the local film as the length of the CDW surpasses a critical value. The pronounced conductivity produced by the sCDW is several orders of magnitude higher than those of previously reported uncharged[9–13] or charged[15,21] domain walls. The resistive change enabled by the sCDW switching presents a much higher off/on ratio for the nondestructive readout than ferroelectric memories of other types, including ferroelectric tunneling junctions[28–30] and switchable ferroelectric diodes.[31,32] Using this effect, ultra-high-density information storage based on sCDWs may be possible, as shown by reports of arrays of sCDWs with a spacing of 10 nm in films produced by molecular-beam epitaxy.[17]

Experimental Section

Film Growth: The (001)$_P$ oriented 20 nm thick BiFeO$_3$ ferroelectric and 20 nm thick epitaxial La$_{0.7}$Sr$_{0.3}$MnO$_3$ electrode films were grown on single crystal (110)$_O$ TbScO$_3$ surfaces by the same molecular-beam epitaxy method described in ref. [17] (subscripts P and O indicate pseudocubic and orthorhombic indices, respectively). The 20 nm thick conducting La$_{0.7}$Sr$_{0.3}$MnO$_3$ buffer layer was deposited at a substrate

temperature (T_{sub}) of 700 °C in a background pressure of 5×10^{-7} Torr in a mixture of O$_2$ + 10% O$_3$[35] and the 20 nm thick BiFeO$_3$ film was deposited at $T_{sub} \approx 625$ °C with a background partial pressure of 1×10^{-6} Torr distilled ozone (≈80% ozone).[36]

TEM: TEM specimens were prepared by mechanical polishing followed by argon ion milling. Ferroelectric domain switching was observed in real time by in situ TEM using a JEOL 3011 operated at 300 kV, with a custom-designed Nanofactory TEM holder with a piezo-driven probe. Electrical voltage was applied between a biased movable tungsten tip and the conductive buffer layer La$_{0.7}$Sr$_{0.3}$MnO$_3$ bottom electrode, which was connected to the holder ground using silver paint.

PFM and SSRM: PFM and SSRM measurements were carried out on an NT-MDT spectra scanning probe microscope using Budget Sensor Pt/Cr-coated tips. The PFM AC signal was applied to the sample with the tip held at ground, and the PFM response was collected near the tip-sample resonance to improve the signal-noise ratio. For switching, a fixed DC bias was applied to the tip during scanning. The spreading resistance was measured immediately after switching.

Supporting Information

Supporting Information is available from the Wiley Online Library or from the author.

[1] J. Mannhart, D. G. Schlom, *Science* **2010**, *327*, 1607.
[2] P. Zubko, S. Gariglio, M. Gabay, P. Ghosez, J. M. Triscone, *Annu. Rev. Condens. Matter Phys.* **2011**, *2*, 141.
[3] S. Thiel, G. Hammerl, A. Schmehl, C. W. Schneider, J. Mannhart, *Science* **2006**, *313*, 1942.
[4] J. Chakhalian, J. W. Freeland, G. Srajer, J. Strempfer, G. Khaliullin, J. C. Cezar, T. Charlton, R. Dalgliesh, C. Bernhard, G. Cristiani, H. U. Habermeier, B. Keimer, *Nat. Phys.* **2006**, *2*, 244.
[5] A. Gozar, G. Logvenov, L. F. Kourkoutis, A. T. Bollinger, L. A. Giannuzzi, D. A. Muller, I. Bozovic, *Nature* **2008**, *455*, 782.

[6] X. K. Wei, A. K. Tagantsev, A. Kvasov, K. Roleder, C. L. Jia, N. Setter, *Nat. Commun.* **2014**, *5*, 3031.

[7] J. Privratska, V. Janovec, *Ferroelectrics* **1997**, *204*, 321.

[8] J. Privratska, V. Janovec, *Ferroelectrics* **1999**, *222*, 23.

[9] J. Seidel, L. W. Martin, Q. He, Q. Zhan, Y. H. Chu, A. Rother, M. E. Hawkridge, P. Maksymovych, P. Yu, M. Gajek, N. Balke, S. V. Kalinin, S. Gemming, F. Wang, G. Catalan, J. F. Scott, N. A. Spaldin, J. Orenstein, R. Ramesh, *Nat. Mater.* **2009**, *8*, 229.

[10] J. Seidel, P. Maksymovych, Y. Batra, A. Katan, S. Y. Yang, Q. He, A. P. Baddorf, S. V. Kalinin, C. H. Yang, J. C. Yang, Y. H. Chu, E. K. H. Salje, H. Wormeester, M. Salmeron, R. Ramesh, *Phys. Rev. Lett.* **2010**, *105*, 197603.

[11] J. Guyonnet, I. Gaponenko, S. Gariglio, P. Paruch, *Adv. Mater.* **2011**, *23*, 5377.

[12] P. Maksymovych, J. Seidel, Y. H. Chu, P. P. Wu, A. P. Baddorf, L. Q. Chen, S. V. Kalinin, R. Ramesh, *Nano Lett.* **2011**, *11*, 1906.

[13] S. Farokhipoor, B. Noheda, *Phys. Rev. Lett.* **2011**, *107*, 127601.

[14] T. Sluka, A. K. Tagantsev, P. Bednyakov, N. Setter, *Nat. Commun.* **2013**, *4*, 1808.

[15] P. Maksymovych, A. N. Morozovska, P. Yu, E. A. Eliseev, Y. H. Chu, R. Ramesh, A. P. Baddorf, S. V. Kalinin, *Nano Lett.* **2012**, *12*, 209.

[16] P. Gao, C. T. Nelson, J. R. Jokisaari, Y. Zhang, S. H. Baek, C. W. Bark, E. Wang, Y. M. Liu, J. Y. Li, C. B. Eom, X. Q. Pan, *Adv. Mater.* **2012**, *24*, 1106.

[17] L. Z. Li, P. Gao, C. T. Nelson, J. R. Jokisaari, Y. Zhang, S. J. Kim, A. Melville, C. Adamo, D. G. Schlom, X. Q. Pan, *Nano Lett.* **2013**, *13*, 5218.

[18] B. M. Vul, G. M. Guro, I. I. Ivanchik, *Ferroelectrics* **1973**, *6*, 29.

[19] M. Y. Gureev, A. K. Tagantsev, N. Setter, *Phys. Rev. B* **2011**, *83*, 184104.

[20] T. Sluka, A. Tagantsev, *US9171602 B2*, **2015**.

[21] R. K. Vasudevan, A. N. Morozovska, E. A. Eliseev, J. Britson, J. C. Yang, Y. H. Chu, P. Maksymovych, L. Q. Chen, V. Nagarajan, S. V. Kalinin, *Nano Lett.* **2012**, *12*, 5524.

[22] A. Crassous, T. Sluka, A. K. Tagantsev, N. Setter, *Nat. Nanotechnol.* **2015**, *10*, 614.

[23] C. L. Jia, S. B. Mi, K. Urban, I. Vrejoiu, M. Alexe, D. Hesse, *Nat. Mater.* **2008**, *7*, 57.

[24] Y. J. Qi, Z. H. Chen, C. W. Huang, L. H. Wang, X. D. Han, J. L. Wang, P. Yang, T. Sritharan, L. Chen, *J. Appl. Phys.* **2012**, *111*, 104117.

[25] W. Y. Wang, Y. L. Tang, Y. L. Zhu, Y. B. Xu, Y. Liu, Y. J. Wang, S. Jagadeesh, X. L. Ma, *Adv. Mater. Interfaces* **2015**, *2*, 1500024.

[26] P. Gao, C. T. Nelson, J. R. Jokisaari, S. H. Baek, C. W. Bark, Y. Zhang, E. G. Wang, D. G. Schlom, C. B. Eom, X. Q. Pan, *Nat. Commun.* **2011**, *2*, 591.

[27] C. T. Nelson, P. Gao, J. R. Jokisaari, C. Heikes, C. Adamo, A. Melville, S. H. Baek, C. M. Folkman, B. Winchester, Y. J. Gu, Y. M. Liu, K. Zhang, E. G. Wang, J. Y. Li, L. Q. Chen, C. B. Eom, D. G. Schlom, X. Q. Pan, *Science* **2011**, *334*, 968.

[28] M. Gajek, M. Bibes, S. Fusil, K. Bouzehouane, J. Fontcuberta, A. E. Barthelemy, A. Fert, *Nat. Mater.* **2007**, *6*, 296.

[29] V. Garcia, S. Fusil, K. Bouzehouane, S. Enouz-Vedrenne, N. D. Mathur, A. Barthelemy, M. Bibes, *Nature* **2009**, *460*, 81.

[30] P. Maksymovych, S. Jesse, P. Yu, R. Ramesh, A. P. Baddorf, S. V. Kalinin, *Science* **2009**, *324*, 1421.

[31] T. Choi, S. Lee, Y. J. Choi, V. Kiryukhin, S. W. Cheong, *Science* **2009**, *324*, 63.

[32] S. Hong, T. Choi, J. H. Jeon, Y. Kim, H. Lee, H. Y. Joo, I. Hwang, J. S. Kim, S. O. Kang, S. V. Kalinin, B. H. Park, *Adv. Mater.* **2013**, *25*, 2339.

[33] C. T. Nelson, B. Winchester, Y. Zhang, S. J. Kim, A. Melville, C. Adamo, C. M. Folkman, S. H. Baek, C. B. Eom, D. G. Schlom, L. Q. Chen, X. Q. Pan, *Nano Lett.* **2011**, *11*, 828.

[34] H. T. Yi, T. Choi, S. G. Choi, Y. S. Oh, S. W. Cheong, *Adv. Mater.* **2011**, *23*, 3403.

[35] C. Adamo, X. Ke, H. Q. Wang, H. L. Xin, T. Heeg, M. E. Hawley, W. Zander, J. Schubert, P. Schiffer, D. A. Muller, L. Maritato, D. G. Schlom, *Appl. Phys. Lett.* **2009**, *95*, 112504.

[36] J. F. Ihlefeld, A. Kumar, V. Gopalan, D. G. Schlom, Y. B. Chen, X. Q. Pan, T. Heeg, J. Schubert, X. Ke, P. Schiffer, J. Orenstein, L. W. Martin, Y. H. Chu, R. Ramesh, *Appl. Phys. Lett.* **2007**, *91*, 071922.